

# Dipole moment surfaces and the mid- and far-IR spectra of N<sub>2</sub>-Ar

Feng Wang<sup>a)</sup>

*School of Chemistry, The University of Melbourne, Victoria 3010, Australia*

Frederick R. W. McCourt<sup>b)</sup> and Robert J. Le Roy<sup>c)</sup>

*Guelph-Waterloo Centre for Graduate Work in Chemistry and Biochemistry, University of Waterloo, Waterloo, Ontario N2L 3G1, Canada*

(Received 23 March 2000; accepted 4 April 2000)

An improved theoretical long-range dispersion plus induction dipole moment surface for N<sub>2</sub>-Ar is presented, and detailed numerical simulations are used to test its predictions against experimental far-IR and mid-IR spectra using two previously-reported potential energy surfaces. As was found in earlier work on the mid-IR spectrum using a pure induction dipole surface, the MMSV<sub>mod</sub> potential of Jäger *et al.* [J. Chem. Soc. Faraday Discuss. **97**, 105 (1994)] yields distinctly better agreement with both experiments than does the XC-3 potential of Dham *et al.* [J. Chem. Phys. **103**, 8477 (1995)]. However, the new dipole surface yields slightly poorer agreement with certain features of the experimental mid-IR and far-IR spectra, which suggests that the existing theoretical values and derivatives with respect to the bond length of some of the permanent moment and (hyper)polarizability properties of N<sub>2</sub> need improvement. © 2000 American Institute of Physics. [S0021-9606(00)00725-X]

## I. INTRODUCTION

Fully resolved infrared (IR) spectra of weakly-bound van der Waals complexes are the best single source of experimental information about both their intermolecular potential energy surfaces and their dipole moment surfaces since the transition frequencies and intensities directly reflect the energies and wavefunctions of individual states, and the range of levels observable in the complete IR spectrum spans the entire attractive potential well. In particular, the positions of the infrared lines allow a highly accurate determination of the attractive region of the potential energy surface, as well as reasonably reliable predictions for the lower energy part of the repulsive wall. An accurate determination of the more strongly repulsive regions of the potential surface requires additional input, such as high quality *ab initio* calculations, linewidth and lineshift data, scattering cross-sections, and a variety of bulk property data. When available, microwave (MW) data allow the properties of the lowest levels, and hence effectively also the position and shape of the potential at its minimum, to be determined quite accurately.

Although N<sub>2</sub>-Ar is one of the first heavy rotor complexes for which discrete IR spectra were observed,<sup>1</sup> even the much more accurate recent IR spectra<sup>2,3</sup> of this system have not yet attained rotational resolution. The interpretation of such incompletely resolved data necessarily relies on comparisons of the experimental results with theoretical simulations of the overall spectral band shape, a process complicated both by the effect on the simulated spectra of inaccuracies in the potential energy and dipole moment surfaces, and by the need to subtract the collision-induced absorption background

continuum from the experimental spectrum. Simulations of unresolved IR spectra are also computationally very demanding, as each observed peak in a partially-resolved spectrum is the sum of many individual transitions, and depends on both the intensities and the distribution of the individual lines. For a complex such as N<sub>2</sub>-Ar, with a relatively large reduced mass and a moderately deep potential well, such calculations are tedious and computationally expensive.<sup>4,5</sup>

Very few realistic simulations of unresolved IR spectra of van der Waals molecules have thus far been carried out. The earliest were those for N<sub>2</sub>-Ar reported by Ayllón *et al.*,<sup>4</sup> whose results first demonstrated the feasibility of generating meaningful predictions of the unresolved IR spectra of moderately heavy complexes. Their pioneering calculations demonstrated the need both for an improved potential energy surface for this system and for a better understanding of the nature of the dipole moment surface governing such spectra. Since their work, which used the Candori *et al.*<sup>6</sup> (CPV) potential energy surface, two newer N<sub>2</sub>-Ar potential surfaces have become available, the MMSV<sub>mod</sub> surface of Jäger *et al.*<sup>7</sup> and the XC-3 potential of Dham *et al.*<sup>8</sup> Both of these potentials are more accurate than the earlier CPV surface in the vicinity of the global minimum, as they were adjusted to give good agreement with the microwave data of Jäger *et al.*<sup>7,9</sup> Comparisons between calculated and experimental bulk properties have shown that these potentials are also superior to the CPV surface in the repulsive region.<sup>8</sup> Following the approach of Ayllón *et al.*,<sup>4</sup> our earlier work on this system reported the results of an essentially exact quantum simulation of the mid- and far-IR spectra, undertaken in order both to study the role of the dipole moment surfaces governing those spectra and to test the more recent MMSV<sub>mod</sub> and XC-3 potential energy surfaces.<sup>5</sup>

The work of Ref. 5 showed that the contributions of the

<sup>a)</sup>Electronic mail: f.wang@chemistry.unimelb.edu.au

<sup>b)</sup>Electronic mail: mccourt@UWaterloo.ca

<sup>c)</sup>Electronic mail: leroy@UWaterloo.ca

short-range terms in the semi-empirical dipole moment surface for <sup>14</sup>N<sub>2</sub>-Ar to the relative intensities of the features of the mid-IR spectrum are negligible, and that the induction contributions dominate the intensities. It also showed that the spectrum generated using the MMSV<sub>mod</sub> potential with the improved model dipole moment surface used there gave better agreement with experiment than did that calculated using the more recent XC-3 surface. This implies that the former is more realistic than the latter, at least in the potential well region to which this property is most sensitive.

When our previous comprehensive simulations of the mid-IR spectrum of <sup>14</sup>N<sub>2</sub>-Ar were in press, a new moderately high resolution far-IR spectrum of N<sub>2</sub>-Ar at  $T=89$  K was reported by Wishnow *et al.*<sup>3</sup> Some features of that spectrum are intriguingly similar to those of the far-IR spectrum we had predicted with a simulation temperature of  $T=77$  K.<sup>5</sup> The objectives of the present work are therefore threefold. First, to test potential and dipole moment surfaces against the new far-IR data; this requires simulations to be performed for the correct temperature using the correct spectral resolution averaging. Second, we wish to present a new theoretical dipole moment surface and to compare its predictions with those yielded by the simple semi-empirical functions used heretofore.<sup>5</sup> Third, we wish to determine whether the difference in the quality of agreement with experiment for spectra generated using the MMSV<sub>mod</sub> and XC-3 potential energy surfaces persists when this more accurate dipole moment surface is employed.

In the present paper, in Sec. II we present our new dipole moment functions governing the mid- and far-IR spectral simulations, while in Sec. III we describe the spectral simulation and the computational procedures employed in the present work. The results obtained from these simulations, and discussions of the radial and angular behavior of the dipole moment function and of the differences between the simulations obtained using the two potential energy surfaces, as well as of the role of the dispersion contributions in the dipole surfaces, are found in Sec. IV. Our conclusions are then presented in Sec. V.

## II. NEW THEORETICAL DIPOLE MOMENT SURFACE FOR N<sub>2</sub>-Ar

### A. General considerations

A body-fixed coordinate system is usually most appropriate for calculating properties of a semi-rigid van der Waals complex with a large potential anisotropy,<sup>10</sup> so it is used here. In the body-fixed coordinate system, the N<sub>2</sub>-Ar complex is assumed to lie in the  $xz$ -plane with the origin located at the diatom center-of-mass. The  $z$ -axis lies along the van der Waals bond axis  $\mathbf{R}$ , while  $\theta$  is the angle between  $\hat{\mathbf{R}}$  and the direction of the N<sub>2</sub> bond axis  $\hat{\mathbf{r}}$ .

The dipole moment of a molecule is a vector function of the nuclear coordinates, a tensor of rank 1. For an atom-diatom van der Waals complex, the dipole moment is denoted  $\boldsymbol{\mu}(\mathbf{R}, \mathbf{r})$ , and its spherical components  $\mu_M(\mathbf{R}, \mathbf{r})$  ( $M=0, \pm 1$ ) in the body-fixed system can be expanded as<sup>10,11</sup>

$$\begin{aligned}\mu_M(\mathbf{R}, \mathbf{r}) &= \sum_{j,K} \mu_{jK}^{\text{BF}}(R, r) \Phi_{jK}^{1M}(\hat{\mathbf{R}}, \hat{\mathbf{r}}) \\ &= \frac{4\pi}{\sqrt{3}} \sum_{j,K} \mu_{jK}^{\text{BF}}(R, r) D_{MK}^1(\alpha, \beta, 0) * \mathcal{Y}_{jK}(\hat{\mathbf{R}}, \hat{\mathbf{r}}),\end{aligned}\quad (1)$$

in which  $\Phi_{jK}^{1M}(\hat{\mathbf{R}}, \hat{\mathbf{r}})$  is a body-fixed basis function,  $D_{MK}^1(\alpha, \beta, \gamma)$  a Wigner rotation function,<sup>12</sup>  $\mathcal{Y}_{jK}(\hat{\mathbf{R}}, \hat{\mathbf{r}})$  is a generalized spherical harmonic,<sup>10</sup> the superscript 1 in various functions indicates the rank of the dipole moment tensor, and the summation includes only functions with odd parity.<sup>10</sup>

The dipole moment of an atom-diatom complex may also be expressed using a space-fixed coordinate system. In particular, if the members of a complete basis set spanning the angular space for an atom-diatom system in a space-fixed coordinate system are designated  $\Psi_{jl}^{JM}(\hat{\mathbf{R}}, \hat{\mathbf{r}})$ , then the spherical components of the dipole moment vector  $\boldsymbol{\mu}$  can also be expanded in the form<sup>10</sup>

$$\mu_M(\mathbf{R}, \mathbf{r}) = \sum_{j,l} \mu_{jl}^{\text{SF}}(R, r) \Psi_{jl}^{1M}(\hat{\mathbf{R}}, \hat{\mathbf{r}}). \quad (2)$$

The summation here is again restricted to terms with  $J=1$ , the rank of the dipole moment tensor, and to terms with  $(j+l)$  odd, as the dipole moment function has odd parity. The radial coefficients in the body-fixed and space-fixed coordinate frames are connected by the relationship<sup>10,11</sup>

$$\begin{aligned}\mu_{jK}^{\text{BF}}(R, r) &= \sum_l (-1)^{j-l-K} \left( \frac{2l+1}{3} \right)^{1/2} \begin{pmatrix} j & l & 1 \\ K & 0 & -K \end{pmatrix} \\ &\quad \times \mu_{jl}^{\text{SF}}(R, r).\end{aligned}\quad (3)$$

In general, dipole moment functions may have contributions from the permanent dipole moments of the monomers forming the complex, as well as from charge overlap, electron exchange, induction, and dispersion. If the monomers have permanent dipole moments, they would normally make the dominant contributions; however, the N<sub>2</sub> monomer has no permanent dipole moment and Ar has no permanent moments of any order. Charge overlap and electron exchange terms are generally expected to be important only at shorter distances than those sampled by bound van der Waals complexes. Moreover, the results of Ref. 5 showed that short-range contributions to the dipole moment have little effect on the simulated N<sub>2</sub>-Ar IR spectra. Thus, the dominant contributions to the dipole moment surface sampled by the N<sub>2</sub>-Ar infrared spectra are expected to be the induction contribution due to interactions of the permanent quadrupole and hexadecapole moments of N<sub>2</sub> with the polarizability of Ar, plus dispersion and back-induction terms.

Bohr and Hunt have derived explicit expressions for the induction and dispersion plus back-induction contributions to the space-fixed dipole moment radial strength functions  $\mu_{jK}^{\text{SF}}(R, r)$  for the case of a homonuclear diatomic molecule interacting with an S-state atom.<sup>13</sup> On adding corresponding terms in their Eqs. (25)–(29) and (54)–(57) and applying the transformation of Eq. (3), one obtains

$$\mu_{00}^{\text{BF}}(R, r) = \mu_{01}^{\text{SF}}(R, r) \equiv c_{00}(r)/R^7, \quad (4)$$

$$\begin{aligned} \mu_{20}^{\text{BF}}(R, r) &= -\sqrt{2/5}\mu_{21}^{\text{SF}}(R, r) + \sqrt{3/5}\mu_{23}^{\text{SF}}(R, r) \\ &= \sqrt{9/5}\alpha^{\text{Ar}}\Theta(r)/R^4 + c_{20}(r)/R^7, \end{aligned} \quad (5)$$

$$\begin{aligned} \mu_{40}^{\text{BF}}(R, r) &= -\sqrt{4/9}\mu_{43}^{\text{SF}}(R, r) + \sqrt{5/9}\mu_{45}^{\text{SF}}(R, r) \\ &= (5/3)\alpha^{\text{Ar}}\Phi(r)/R^6 + c_{40}(r)/R^7, \end{aligned} \quad (6)$$

$$\begin{aligned} \mu_{21}^{\text{BF}}(R, r) &= -\sqrt{3/10}\mu_{21}^{\text{SF}}(R, r) - \sqrt{2/10}\mu_{23}^{\text{SF}}(R, r) \\ &= -\sqrt{3/5}\alpha^{\text{Ar}}\Theta(r)/R^4 + c_{21}(r)/R^7, \end{aligned} \quad (7)$$

$$\begin{aligned} \mu_{41}^{\text{BF}}(R, r) &= -\sqrt{5/18}\mu_{43}^{\text{SF}}(R, r) - \sqrt{2/9}\mu_{45}^{\text{SF}}(R, r) \\ &= -\sqrt{10/9}\alpha^{\text{Ar}}\Phi(r)/R^6 + c_{41}(r)/R^7, \end{aligned} \quad (8)$$

in which  $\alpha^{\text{Ar}}$  is the polarizability of the Ar atom,  $\Theta = \Theta(r)$  and  $\Phi = \Phi(r)$  are, respectively, the permanent quadrupole and hexadecapole moments of  $\text{N}_2$ , and the  $c_{ij}(r)$ -coefficients are

$$c_{00}(r) = (6/5)\alpha^{\text{Ar}}\Delta\alpha\Theta + 2C_6^{(0)}(r)(\bar{\mathbf{B}}/\bar{\alpha} - \mathbf{B}^{\text{Ar}}/\alpha^{\text{Ar}}), \quad (9)$$

$$\begin{aligned} c_{20}(r) &= \sqrt{4/5} \left[ (3/7)\alpha^{\text{Ar}}(4\alpha_{zz} + 3\alpha_{xx})\Theta + C_6^{(2)}(r) \right. \\ &\quad \left. \times \left( \frac{4\mathbf{B}_{2b} + 12\mathbf{B}_{2c}}{\Delta\alpha} - \frac{\mathbf{B}^{\text{Ar}}}{\alpha^{\text{Ar}}} \right) \right], \end{aligned} \quad (10)$$

$c_{40}(r)$

$$\begin{aligned} &= (16/15) \left[ (3/7)\alpha^{\text{Ar}}\Delta\alpha\Theta \right. \\ &\quad \left. + \frac{35C_8^{(4)}(r)\mathbf{B}_4}{9(2\mathbf{C}_{zz,zz} - 4\mathbf{C}_{xz,xz} + \mathbf{C}_{xx,xx}) + 5(\mathbf{E}_{z,zzz} + 2\mathbf{E}_{x,xxx})} \right], \end{aligned} \quad (11)$$

$$\begin{aligned} c_{21}(r) &= \sqrt{3/5} \left[ (1/7)\alpha^{\text{Ar}}(6\alpha_{zz} + \alpha_{xx})\Theta + (1/3)C_6^{(2)}(r) \right. \\ &\quad \left. \times \left( \frac{4\mathbf{B}_{2b} + 20\mathbf{B}_{2c}}{\Delta\alpha} + \frac{\mathbf{B}^{\text{Ar}}}{\alpha^{\text{Ar}}} \right) \right], \end{aligned} \quad (12)$$

$$c_{41}(r) = \sqrt{5/8}c_{40}(r). \quad (13)$$

In these expressions  $\alpha_{ij}$  is the  $ij$ -th element of the (dipole) polarizability tensor of  $\text{N}_2$ ,  $\bar{\alpha}$  is its spherical average, and  $\Delta\alpha = \alpha_{zz} - \alpha_{xx}$  its anisotropy, while the  $C_n^{(\lambda)}$  are the leading angular dispersion coefficients of the  $\text{N}_2$ -Ar van der Waals interaction energy,

$$\begin{aligned} V_{\text{vdW}}(R, r, \theta) &= -[C_6^{(0)}(r) + C_6^{(2)}(r)P_2(\cos\theta)]/R^6 \\ &\quad - [C_8^{(0)}(r) + C_8^{(2)}(r)P_2(\cos\theta) \\ &\quad + C_8^{(4)}(r)P_4(\cos\theta)]/R^8. \end{aligned} \quad (14)$$

Similarly,  $\mathbf{B}^{\text{Ar}}$  is the isotropic mixed dipole-dipole-quadrupole hyperpolarizability of Ar, the  $\mathbf{C}_{ij,kl}$  and  $\mathbf{E}_{i,jkl}$  factors are Cartesian components of the fourth-rank quadrupole and dipole-octopole polarizability tensors  $\mathbf{C}$  and  $\mathbf{E}$  of

$\text{N}_2$ , while  $\bar{\mathbf{B}}$  is the spherical average and  $\mathbf{B}_{2b}$ ,  $\mathbf{B}_{2c}$ , and  $\mathbf{B}_4$  are linear combinations of the Cartesian components  $\mathbf{B}_{ij,kl}$  of the fourth-rank mixed dipole-dipole-quadrupole hyperpolarizability tensor  $\mathbf{B}$  of  $\text{N}_2$ , namely,

$$\bar{\mathbf{B}} = (2/15)(\mathbf{B}_{zz,zz} + 4\mathbf{B}_{xz,xz} + \mathbf{B}_{xx,zz} + 4\mathbf{B}_{xx,xx}), \quad (15)$$

$$\mathbf{B}_{2b} = (1/42)(3\mathbf{B}_{zz,zz} - 8\mathbf{B}_{xz,xz} + 26\mathbf{B}_{xx,zz} + 16\mathbf{B}_{xx,xx}), \quad (16)$$

$$\mathbf{B}_{2c} = (1/14)(\mathbf{B}_{zz,zz} + 2\mathbf{B}_{xz,xz} - 3\mathbf{B}_{xx,zz} - 4\mathbf{B}_{xx,xx}), \quad (17)$$

$$\mathbf{B}_4 = (1/70)(3\mathbf{B}_{zz,zz} - 8\mathbf{B}_{xz,xz} - 2\mathbf{B}_{xx,zz} + 2\mathbf{B}_{xx,xx}). \quad (18)$$

The fact that  $\mathbf{B}_{xz,xz} = \mathbf{B}_{zx,zx}$  for the zero-frequency susceptibilities simplifies Eqs. (12)–(16) of Ref. 13, and makes their  $\mathbf{B}_{2d} = \mathbf{B}_{2c}$ . Note that while all of these properties of  $\text{N}_2$  in general depend on its bond length  $r$ , for the sake of compactness this dependence is not explicitly shown in most terms on the right hand sides of Eqs. (9)–(13).

## B. Effective dipole moment functions for the far-IR and mid-IR spectra

Infrared transitions of the  $\text{N}_2$ -Ar complex in general involve changes in both the van der Waals and the diatom vibrotor states. However, while motion involving the van der Waals bond length  $R$  and the angular coordinate  $\theta$  are strongly coupled, the diatom stretching vibration is orders of magnitude faster, and is approximately adiabatically separable from the angular and radial van der Waals motions. As a result, it is usually a good approximation to represent the total system wavefunction as the product of a strongly-coupled function of  $R$  and  $\theta$  with the vibrational radial wavefunction of a free  $\text{N}_2$  molecule. This assumption is implicit in all quantitative treatments of van der Waals molecule dynamics over the past 25 years,<sup>10,14</sup> and is the basis for the description of different effective two-dimensional potentials for atom-diatom van der Waals molecules formed from diatomic molecules in different vibration-rotation states.<sup>14–17</sup>

The  $\mu_{jK}^{\text{BF}}(R, r)$  radial strength functions may in general be expanded as a Taylor series about a reference diatom bond length  $r_0$  as

$$\begin{aligned} \mu_{jK}^{\text{BF}}(R, r) &= \mu_{jK}^{\text{BF}}(R, r_0) + (r - r_0) \left( \frac{d\mu_{jK}^{\text{BF}}(R, r)}{dr} \right)_{r_0} \\ &\quad + \frac{(r - r_0)^2}{2} \left( \frac{d^2\mu_{jK}^{\text{BF}}(R, r)}{dr^2} \right)_{r_0} + \dots \end{aligned} \quad (19)$$

Within the adiabatic separability approximation described above, the components of the effective dipole moment function which govern transitions between states associated with  $\text{N}_2$  vibrational quantum numbers  $v'$  and  $v''$  are

$$\begin{aligned} \bar{\mu}_{jK}^{\text{BF}}(R; v', v'') &= \langle v' | \mu_{jK}^{\text{BF}}(R, r) | v'' \rangle = \mu_{jK}^{\text{BF}}(R, r_0) \langle v' | v'' \rangle \\ &\quad + \mu_{jK}^{\text{BF}}(R, r_0)' \langle v' | r - r_0 | v'' \rangle + \dots, \end{aligned} \quad (20)$$

where  $\mu_{jK}^{\text{BF}}(R, r_0)' \equiv (d\mu_{jK}^{\text{BF}}(R, r)/dr)_{r_0}$ , and  $|v''\rangle$  and  $|v'\rangle$ , respectively, represent the lower- and upper-state diatom ra-

dial wavefunctions. Since  $\langle v' | v'' \rangle = \delta_{v', v''}$  and  $\langle v'' | r - r_0 | v' \rangle$  is very small unless  $|v'' - v'| = 1$ , the first term in Eq. (20) provides the dominant contribution to the far-IR spectrum (for which  $v' = v'' = 0$ ) and the second provides the dominant term for the mid-IR spectrum (for which  $v' = v'' + 1 = 1$ ). In other words, the far-IR and mid-IR spectra are driven by two different effective two-dimensional ( $R, \theta$ ) surfaces, the former by the first term on the right hand side of Eq. (20) and the latter by the second term.

From Eqs. (1) and (20), the spherical components of the effective dipole moment function driving the IR transitions may be written as

$$\begin{aligned} \bar{\mu}_M^{v'v''}(R, \theta) &\equiv \langle v' | \mu_M(\mathbf{R}, \mathbf{r}) | v'' \rangle \\ &= (4\pi/\sqrt{3}) \sum_{j,K} \bar{\mu}_{jK}^{\text{BF}}(R; v', v'') \\ &\quad \times D_{MK}^1(\alpha, \beta, 0) * \mathcal{Y}_{jK}(\hat{\mathbf{R}}, \hat{\mathbf{r}}). \end{aligned} \quad (21)$$

In the body-fixed frame the effective dipole-moment functions collapse to the simple sums of products of radial and angular functions required for the intensity calculations,<sup>18</sup>

$$\begin{aligned} \bar{\mu}_z^{v'v''}(R, \theta) &= \sum_j \bar{\mu}_{j0}^{\text{BF}}(R; v', v'') P_j^0(\cos \theta), \\ \bar{\mu}_x^{v'v''}(R, \theta) &= \sum_j \bar{\mu}_{j1}^{\text{BF}}(R; v', v'') P_j^1(\cos \theta), \end{aligned} \quad (22)$$

where the  $P_j^{m_l}(\cos \theta)$  are associated Legendre polynomials. Thus, the components of the effective dipole moment function driving the far-IR spectrum of N<sub>2</sub>-Ar which is due to transitions between states in which the N<sub>2</sub> monomer remains in its ground vibrational state ( $v' = v'' = 0$ ), have the forms

$$\begin{aligned} \mu_z^{\text{fIR}}(R, \cos \theta) &= [c_{00}(r_0)/R^7] P_0^0(\cos \theta) \\ &\quad + [(3/\sqrt{5})\alpha^{\text{Ar}}\Theta(r_0)/R^4 \\ &\quad + c_{20}(r_0)/R^7] P_2^0(\cos \theta) \\ &\quad + [(5/3)\alpha^{\text{Ar}}\Phi(r_0)/R^6 \\ &\quad + c_{40}(r_0)/R^7] P_4^0(\cos \theta), \end{aligned} \quad (23)$$

$$\begin{aligned} \mu_x^{\text{fIR}}(R, \cos \theta) &= [-\sqrt{3/5}\alpha^{\text{Ar}}\Theta(r_0)/R^4 \\ &\quad + c_{21}(r_0)/R^7] P_2^1(\cos \theta) \\ &\quad + [-\sqrt{10/9}\alpha^{\text{Ar}}\Phi(r_0)/R^6 \\ &\quad + c_{41}(r_0)/R^7] P_4^1(\cos \theta), \end{aligned} \quad (24)$$

where the various properties of N<sub>2</sub> are evaluated at the chosen reference distance  $r = r_0$ .

The mid-IR spectrum of a van der Waals complex is due to transitions among vibration-rotation states associated with the van der Waals modes plus a  $v'' = 0 \rightarrow v' = 1$  transition of the N<sub>2</sub> monomer. As a result, the effective dipole moment functions governing such transitions are determined by the expansion coefficients  $\bar{\mu}_{jk}^{\text{BF}}(R; 1, 0)$ , which in turn are dominated by the second term on the right hand side of Eq. (20). The components of the transition dipole moment function appropriate for mid-IR simulations thus have the forms

TABLE I. Parameters determining the components of the N<sub>2</sub>-Ar dipole moment surfaces for  $r = r_0 = 2.02726a_0$ . Unless otherwise specified, results are from Ref. 19.

Parameter/a.u.	Value	Radial derivative <sup>a</sup>
$\Theta/ea_0^2$	-0.96803	1.15 <sup>b</sup>
$\Phi/ea_0^4$	-6.95282	-2.53 <sup>b</sup>
$\alpha_{zz}/e^2a_0^2E_h^{-1}$	14.343	12.08
$\alpha_{xx}/e^2a_0^2E_h^{-1}$	9.524	4.40
$\bar{\alpha}/e^2a_0^2E_h^{-1}$	11.130	6.96
$\Delta\alpha/e^2a_0^2E_h^{-1}$	4.819	7.68
$B_{zz,zz}/e^3a_0^4E_h^{-2}$	-180	-112.5
$B_{zz,xz}/e^3a_0^4E_h^{-2}$	-108	-91.26
$B_{xx,zz}/e^3a_0^4E_h^{-2}$	59	101.1
$B_{xx,xx}/e^3a_0^4E_h^{-2}$	-94	-108.0
$C_{zz,zz}/e^2a_0^4E_h^{-1}$	30.16	17.61
$C_{xz,xz}/e^2a_0^4E_h^{-1}$	23.20	14.21
$C_{xx,xx}/e^2a_0^4E_h^{-1}$	14.67	7.00
$E_{z,zzz}/e^2a_0^4E_h^{-1}$	28.65	13.66
$E_{x,xxx}/e^2a_0^4E_h^{-1}$	-17.31	-2.86
$C_6^{(0)}/a_0^6E_h$	64.766 <sup>c</sup>	15.35 <sup>c</sup>
$C_6^{(2)}/a_0^6E_h$	5.469 <sup>c</sup>	1.74 <sup>c</sup>
$C_8^{(4)}/a_0^8E_h$	-40.888 <sup>c</sup>	67.85 <sup>c</sup>
$B^{\text{Ar}}/e^3a_0^4E_h^{-2}$	-131 <sup>d</sup>	...
$\alpha^{\text{Ar}}/e^2a_0^4E_h^{-1}$	11.062 <sup>d</sup>	...

<sup>a</sup>Radial derivatives are with respect to distance in  $a_0$ .

<sup>b</sup>From Ref. 19.

<sup>c</sup>From Ref. 20. Values and radial derivatives of  $C_n^{(\lambda)}$  at  $r_0 = 2.02726a_0$  were obtained from linear fits to the calculated values at  $r = 1.968, 2.068$ , and  $2.168a_0$ .

<sup>d</sup>From Ref. 21.

$$\begin{aligned} \mu_z^{\text{mIR}}(R, \cos \theta) &= \langle 1 | r - r_0 | 0 \rangle \{ [c_{00}'(r_0)/R^7] P_0^0(\cos \theta) \\ &\quad + [(3/\sqrt{5})\alpha^{\text{Ar}}\Theta'(r_0)/R^4 \\ &\quad + c_{20}'(r_0)/R^7] P_2^0(\cos \theta) \\ &\quad + [(5/3)\alpha^{\text{Ar}}\Phi'(r_0)/R^6 \\ &\quad + c_{40}'(r_0)/R^7] P_4^0(\cos \theta) \}, \end{aligned} \quad (25)$$

$$\begin{aligned} \mu_x^{\text{mIR}}(R, \cos \theta) &= \langle 1 | r - r_0 | 0 \rangle \{ [-\sqrt{3/5}\alpha^{\text{Ar}}\Theta'(r_0)/R^4 \\ &\quad + c_{21}'(r_0)/R^7] P_2^1(\cos \theta) \\ &\quad + [-\sqrt{10/9}\alpha^{\text{Ar}}\Phi'(r_0)/R^6 \\ &\quad + c_{41}'(r_0)/R^7] P_4^1(\cos \theta) \}. \end{aligned} \quad (26)$$

These expressions are clearly analogous to Eqs. (23) and (24), except that each term representing a property of the N<sub>2</sub> monomer is replaced by its derivative with respect to  $r$  (evaluated at  $r_0$ ), and the functions are premultiplied by the diatomic molecule vibrational matrix element  $\langle 1 | r - r_0 | 0 \rangle$ .

Values for the properties of N<sub>2</sub> and Ar appearing in Eqs. (4)–(18) obtained from *ab initio* calculations are listed in Table I; those for N<sub>2</sub> were calculated for  $r_0 = 1.07278 \text{ \AA}$ . This value of  $r_0$  is the *ab initio* equilibrium bond length at the level of theory used for most of the property calculations,<sup>22</sup> and while it is slightly smaller than either the experimental<sup>23</sup>  $r_e = 1.09768 \text{ \AA}$  or the average bond length in the ground state  $\bar{r}_{v''=0} = 1.10148 \text{ \AA}$ , it seemed best to use these internally consistent results for which symmetric first differences yield the radial derivatives of the properties. The

TABLE II. Legendre contributions to  $x$ - and  $z$ -components of dipole moment vectors, in atomic units.

Far-IR coefficients		Mid-IR coefficients		$R$ -factor	$\theta$ -factor
Term	Value	Term	Value		
$c_{00}$	30.47	$c_{00}'$	-356.3	$R^{-7}$	$P_0^0(\cos \theta)$
$\sqrt{9/5}\alpha^{Ar}\Theta$	-14.37	$\sqrt{9/5}\alpha^{Ar}\Theta'$	17.07	$R^{-4}$	$P_2^0(\cos \theta)$
$c_{20}$	-432.0	$c_{20}'$	340.4	$R^{-7}$	$P_2^0(\cos \theta)$
$(5/3)\alpha^{Ar}\Phi$	-128.2	$(5/3)\alpha^{Ar}\Phi'$	-46.64	$R^{-6}$	$P_2^0(\cos \theta)$
$c_{40}$	-21.53	$c_{40}'$	-16.31	$R^{-7}$	$P_4^0(\cos \theta)$
$-\sqrt{3/5}\alpha^{Ar}\Theta$	8.295	$-\sqrt{3/5}\alpha^{Ar}\Theta'$	-9.854	$R^{-4}$	$P_2^1(\cos \theta)$
$c_{21}$	-202.6	$c_{21}'$	97.23	$R^{-7}$	$P_2^1(\cos \theta)$
$-\sqrt{10/9}\alpha^{Ar}\Phi$	81.07	$-\sqrt{10/9}\alpha^{Ar}\Phi'$	29.50	$R^{-6}$	$P_2^1(\cos \theta)$
$c_{41}$	-17.02	$c_{41}'$	-12.89	$R^{-7}$	$P_4^1(\cos \theta)$

factors obtained on combining these terms to yield the various coefficients of our working dipole moment expressions, Eqs. (24)–(26), are then summarized in Table II. As in Ref. 5, the value used for  $\langle 1|r-r_0|0\rangle = \langle 1|r|0\rangle = 0.060556a_0$  was calculated from a numerical potential generated from the spectroscopic constants<sup>23</sup> for  $^{14}\text{N}_2$ .

### III. SPECTRAL SIMULATION AND COMPUTATIONAL DETAILS

The mid- and far-infrared spectra of  $^{14}\text{N}_2\text{-Ar}$  were simulated following the procedure described in Ref. 5. First, the eigenvalues and eigenfunctions of all bound states of the complex were calculated using a chosen potential energy surface. Second, subject to the appropriate rotational selection rules, the associated transition intensities or line strengths  $S(f \leftarrow i)$  were calculated using the appropriate dipole moment functions for all possible combinations of all truly bound initial and final states of the complex. This included states with total rotational angular momentum quantum number up to and including  $J=34$ , and yielded a mid-IR spectrum consisting of over 111,000 transitions among some 2,000 bound states; for the far-IR spectrum the number of individual transitions is roughly halved.

In the third step, a fully-resolved simulated spectrum was generated from the integrated intensities for the dipole-allowed transitions,  $I(\nu_{fi})$ , each incorporating the appropriate thermal weight factor,<sup>4,18</sup>

$$I(\nu_{fi}) = 8\pi^3 \nu_{fi} g_i [\exp(-E_i/k_B T) - \exp(-E_f/k_B T)] S(f \leftarrow i) / 3hcQ(T), \quad (27)$$

where  $E_i$  and  $E_f$  are the initial and final state energies,  $\nu_{fi} \equiv E_f - E_i$ ,  $g_i$  is the nuclear spin degeneracy of the initial state,  $Q(T)$  the canonical partition function, and  $k_B$  Boltzmann's constant. Finally, the overall spectral profile was generated from the fully-resolved spectrum by assigning a characteristic lineshape, representative of the type of line broadening appropriate to a bulk gas spectrum at the experimental temperature and pressure, and summing the contributions from the complete set of broadened lines.

As in our previous work,<sup>5</sup> a Lorentzian lineshape function was used to describe the broadening of the spectral lines, which is mainly due to collision broadening. The simulations of the mid-IR spectrum were performed for  $T=77$  K, with

an assumed linewidth (full width at half-maximum) of  $0.20 \text{ cm}^{-1}$ , the conditions associated with McKellar's experiment,<sup>2</sup> while the far-IR simulation were performed for the Wishnow *et al.*<sup>3</sup> experimental temperature of  $T=89$  K and a linewidth of  $0.24 \text{ cm}^{-1}$ .

Two sets of simulations were performed. The objective of the first was to compare results yielded by two different potential energy surfaces, the  $\text{MMSV}_{\text{mod}}$  surface of Ref. 7 and the XC-3 surface of Ref. 8, using our new theoretical dipole moment surface, which includes both induction and dispersion contributions. The objective of the second set of simulations was to determine the contributions associated with the induction part of the dipole surface. They used only the  $\text{MMSV}_{\text{mod}}$  surface, which has been found<sup>5</sup> to yield better agreement with the experimental mid-IR spectrum.<sup>2</sup>

As in Ref. 5, the vibration-rotation eigenstates were determined using the TRIATOM program suite of Tennyson *et al.*<sup>18</sup> Atom-diatom scattering coordinates were used, and  $\text{N}_2$  was assumed to be a rigid molecule with rotational energy levels defined by the experimental<sup>20</sup> inertial rotational constant  $B_0 = 1.989574 \text{ cm}^{-1}$  for the ground vibrational level of the free diatom. The radial basis set consists of 40 Morse-oscillator-like functions defined by the Morse function parameters  $R_e = 11.6a_0$ ,  $D_e = 8.5 \times 10^{-5} E_h$ , and  $\omega_e = 2.2 \times 10^{-5} E_h$ .<sup>5</sup> The physical constants and atomic masses (for  $^{14}\text{N}$  and  $^{40}\text{Ar}$ ) used were taken from Ref. 24:  $m(^{40}\text{Ar}) = 39.9623837 \text{ u}$  and  $m(^{14}\text{N}) = 14.003074002 \text{ u}$ .

### IV. RESULTS AND DISCUSSION

Figure 1 compares the angular behavior of the  $z$ - and  $x$ -components of our new theoretical effective  $\text{N}_2\text{-Ar}$  dipole moment functions (solid curves) with those of the semi-empirical "pure induction dipole" (DIP-4) functions recommended in Ref. 5 (dashed curves) for  $R=3.70 \text{ \AA}$ , the position of the van der Waals potential minimum. Similarly, Fig. 2 compares the radial behavior of the same functions at  $\theta = 75^\circ$ , an angle chosen because none of the functions is near zero there. Note that the "pure induction dipole" (DIP-4) function of Ref. 5 may be obtained from the "full dipole surface" introduced above by neglecting all of the  $c_{ij}(r_0)$  and  $c_{ij}'(r_0)$  dispersion plus back-induction terms.

Figure 1 shows that while the effective dipole functions driving the mid-IR and far-IR spectra have opposite sign, they have approximately the same strength and oscillatory behavior. Of course, the absolute intensity for the mid-IR spectrum will also include both the square of the  $\text{N}_2$  matrix element  $\langle v=1|r|v=0\rangle = 0.060556a_0$ , the frequency factor in Eq. (27) which gives rise to an enhancement of *ca.* 2330/30 at the predicted far-IR intensity maximum, and the population difference factor which further enhances the mid-IR transitions relative to those in the far-IR. Taken together, these considerations imply that the mid-IR and far-IR absorption coefficients should have roughly the same magnitude.

Figure 3 compares simulated 77 K mid-IR spectra of  $\text{N}_2\text{-Ar}$  generated from the  $\text{MMSV}_{\text{mod}}$  potential energy surface<sup>7</sup> (second spectrum from the top) and the XC-3 potential<sup>8</sup> (bottom spectrum) using the new "full dipole surface" of Eqs. (25) and (26) with one another, with McKel-

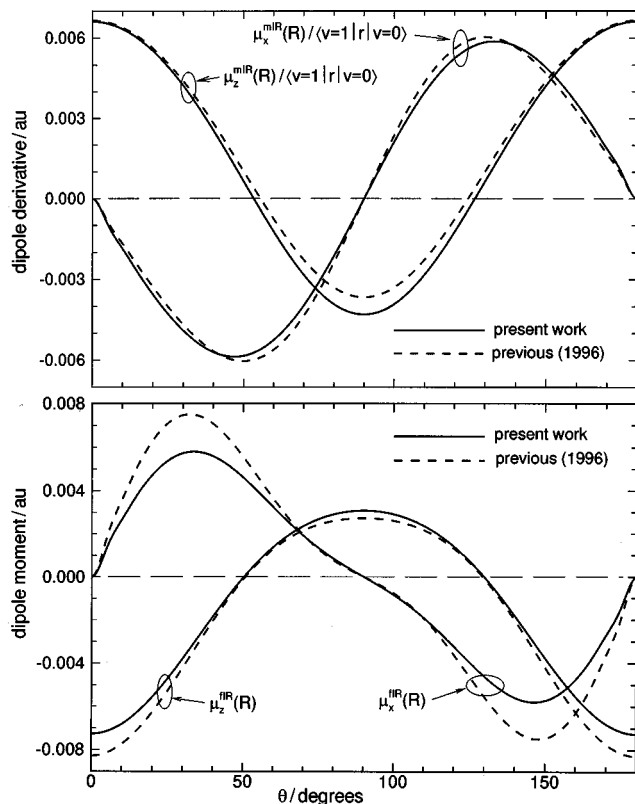


FIG. 1. Angle dependence of the *x*- and *z*-components of the effective dipole moment functions employed for simulations of the mid-IR (upper segment) and far-IR (lower segment) infrared spectra of N<sub>2</sub>-Ar using the full dipole moment surface of Eqs. (23)–(26) (solid curves) or the pure induction dipole function of Ref. 5 (dashed curves) at a van der Waals bond length of  $R = 3.70 \text{ \AA}$  (Ref. 25).

lar's experimental spectrum<sup>2</sup> (second curve from the bottom), and with a spectrum generated from the MMSV<sub>mod</sub> potential using the simpler "pure induction dipole" function of Ref. 5.<sup>25</sup> It is clear that the synthetic mid-IR spectrum generated from the MMSV<sub>mod</sub> potential using the new "full dipole surface" is much closer to experiment than is that generated from the XC-3 potential with the same dipole surface. These results therefore reaffirm our previous conclusion<sup>5</sup> that the MMSV<sub>mod</sub> potential is more realistic than the XC-3 potential in the potential well region.

A prominent difference between the experimental and calculated spectra shown in Fig. 3 is that all three of the simulated spectra have a sharp narrow peak at the band center,  $\nu_0 = 2329.50 \text{ cm}^{-1}$ , while the experimental spectrum has only a broad bump slightly to the red of  $\nu_0$ . This apparent discrepancy is an artifact associated with our use of two-dimensional (rigid-diatom) potential energy surfaces which are identical for complexes formed from N<sub>2</sub>( $v=0$ ) and N<sub>2</sub>( $v=1$ ). As a result, the predicted wavenumbers for all transitions in which the only quantum numbers changing are  $\nu(\text{N}_2)$  and the parity all pile up very near the band center. In the real molecule, however, the N<sub>2</sub>( $v=1$ )-Ar potential is slightly different than that for N<sub>2</sub>( $v=0$ )-Ar, and the associated upper-state levels tend to be shifted by different amounts, so the overall peak broadens out, while retaining approximately the same area, and shifts slightly to the red, since the upper-state levels are usually slightly more strongly

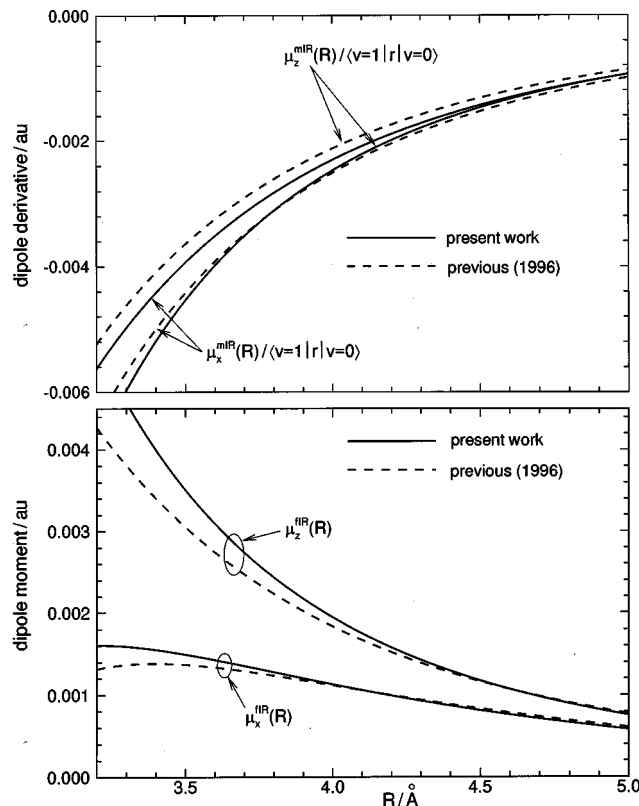


FIG. 2. Cuts for  $\theta = 75^\circ$  showing the radial dependence of the *x*- and *z*-components of the effective dipole moment functions employed for simulations of the mid-IR (upper segment) and far-IR (lower segment) infrared spectra of N<sub>2</sub>-Ar using the full dipole moment surface of Eqs. (23)–(26) (solid curves) or the pure induction dipole function of Ref. 5 (dashed curves) (Ref. 25).

bound. Thus, this apparent discrepancy is readily understood as being the main observable manifestation (other than the  $-0.41 \text{ cm}^{-1}$  shift of  $\nu_0$  from the free molecule vibrational energy<sup>23</sup>) of the diatom bond-length dependence of the potential energy surface.

The two mid-IR spectra calculated using the MMSV<sub>mod</sub> potential (the upper two curves in Fig. 3) are clearly very similar, the main difference being the fact that the relative amplitude of the two broad peaks lying  $\pm 2 \text{ cm}^{-1}$  from the band center at  $2329.50 \text{ cm}^{-1}$  is much greater for the full dipole moment function that was the case for the pure induction dipole. While not shown here, the same conclusion is reached on comparing the bottom curve with a simulated spectrum calculated using the XC-3 potential and the pure induction dipole function. In other words, for both potential energy surfaces this feature of the spectra calculated using the "full dipole moment" function is in poorer agreement with experiment than are the corresponding results obtained using the "pure induction" dipole function. For the XC-3 surface, use of this full dipole surface also has the effect of reducing the relative importance of the narrow simulated peak at the band center (discussed above), but this minor change does not modify the above conclusion. Thus, the change in the relative amplitude of the broad peaks bracketing the band center is entirely due to the strengths of the theoretical  $c_{ij}'(r_0)$  coefficients in Eqs. (25) and (26) relative to those of the  $R^{-4}$ - and  $R^{-6}$ -dependent pure induction

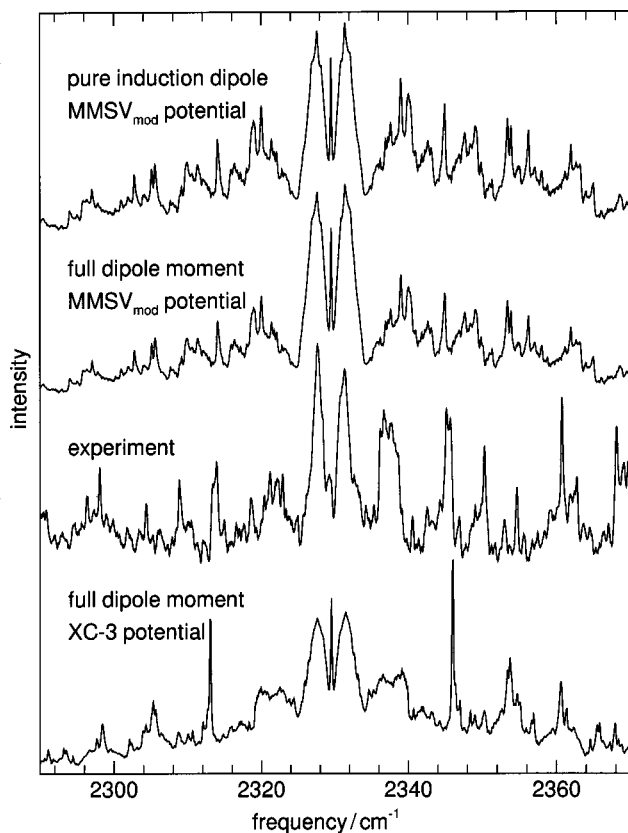


FIG. 3. A comparison of simulated mid-IR spectra of  $N_2$ -Ar at  $T=77$  K calculated using the indicated combinations of potential energy and dipole moment surfaces, with each other, and with experiment (Ref. 2).

terms. It therefore appears that obtaining better agreement with experiment in this region of the spectrum will require improved theoretical values for the “mid-IR coefficient” properties listed in Table II.

Figure 4 compares the 89 K far-IR spectra generated from the same set of potential energy and dipole moment surfaces considered in Fig. 3, with each other, and with the experimental results of Wishnow *et al.*<sup>3</sup> The experimental spectrum is that associated with the middle curve on their Fig. 2, which the experimental conditions ( $P_{N_2}/P_{Ar}=24/76$  and density of 3.04 amagat) suggest should be the best resolved. Although the fine structure in the experimental spectrum for  $\nu \leq 30$   $cm^{-1}$  is increasingly contaminated with noise,<sup>26</sup> that for larger energies is fairly well defined. However, since our simulations consider only truly-bound states of these complexes, they do not show the increasingly smooth large-amplitude “ripple” structure seen in the experimental far-IR spectra for  $\nu \geq 45$   $cm^{-1}$  and in the mid-IR spectra at frequencies more than 45  $cm^{-1}$  from the band center. This loss of structure occurs because those transitions involve states in which the  $N_2$  is relatively highly rotationally excited and associated levels of the complex are metastable with respect to predissociation by internal rotation, which substantially broadens all their transitions. Thus, the far-IR region for the clearest comparisons between theory and experiment is  $30 < \nu < 45$   $cm^{-1}$ . On this interval it is again clear that the MMSV<sub>mod</sub> potential yields more realistic predictions than does the XC-3 surface, which further reaf-

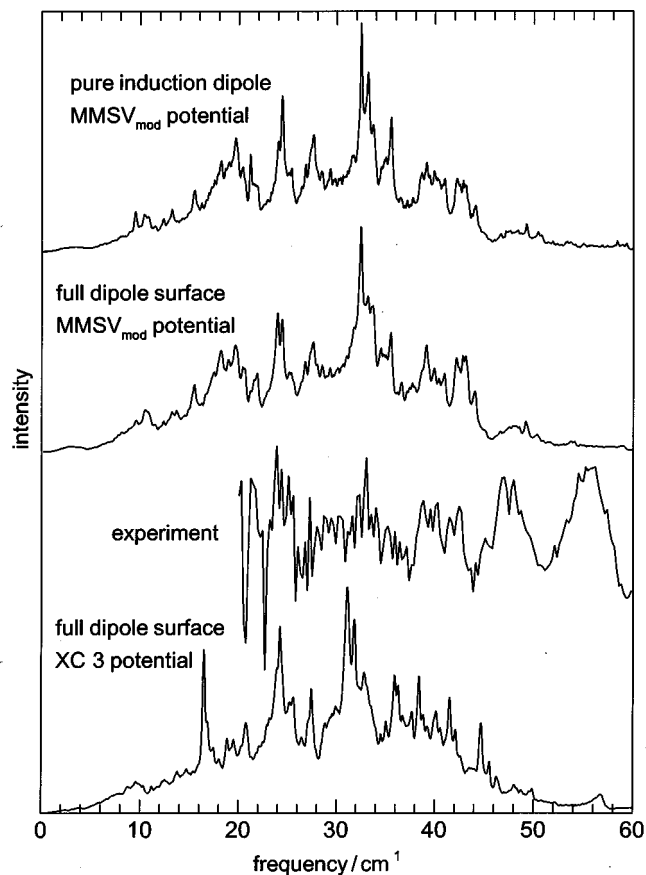


FIG. 4. A comparison of simulated far-IR spectra of  $N_2$ -Ar at  $T=89$  K calculated using the indicated combinations of potential energy and dipole moment surfaces, with each other, and with experiment (Ref. 3).

firms our conclusion regarding the relative merits of these two surfaces in the well region.

While the far-IR spectra generated from the MMSV<sub>mod</sub> potential surface (the top two curves in Fig. 4) are generally quite similar, the structure generated using the “pure induction” dipole function seems in slightly better agreement with experiment in the  $38 < \nu < 45$   $cm^{-1}$  region. This improvement is not large enough to allow a strong statement regarding the quality of one dipole surface over the other, but it does strengthen our concern regarding the accuracy of the *ab initio* properties of  $N_2$  used to define our new full dipole moment surface.

## V. CONCLUSIONS

In the present work we report on an improved theoretical long-range dispersion plus induction dipole moment surface for  $N_2$ -Ar, and test its predictions against far-IR and mid-IR experimental spectra using two previously-reported potential energy surfaces. In agreement with the conclusions of our earlier work on the mid-IR spectrum using a pure induction dipole surface, the MMSV<sub>mod</sub> potential of Ref. 7 yields distinctly better agreement with both experiments than does the XC-3 potential of Ref. 8. However, poorer agreement for the relative amplitude of the large peaks near the mid-IR band origin and certain features of the far-IR spectrum suggests

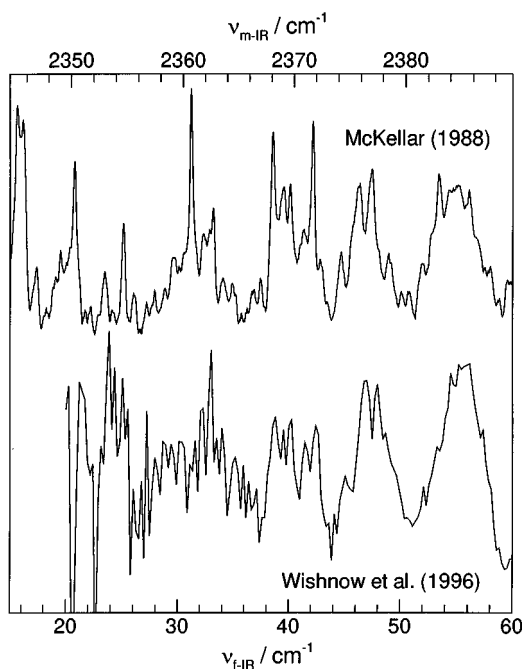


FIG. 5. A comparison of the experimental mid-IR (upper curve and axis) and far-IR (lower curve and axis) spectra, shifted to make the band origins coincide.

that there may be some deficiencies in the existing *ab initio* values of the permanent moment and (hyper)polarizability properties of N<sub>2</sub> listed in Table I.

Aside from the narrow peak at the band center in the simulated mid-IR spectrum (discussed above), both the mid-IR and far-IR spectra generated from the MMSV<sub>mod</sub> potential are in reasonable agreement with experiment. This leads to the following conclusions. (1) The diatom stretching dependence of the potential energy surface for this system does not significantly affect the shapes of these spectra, since the potential energy surface, and hence the bound-state calculations, assume a rigid N<sub>2</sub> molecule. This point is further illustrated by the remarkable qualitative similarity for  $\nu_{f-IR} > 30 \text{ cm}^{-1}$  seen in Fig. 5, which compares the two experimental spectra, displaced so that their band origins coincide.<sup>27</sup> The increasing disparity seen there for  $\nu_{f-IR} \lesssim 30 \text{ cm}^{-1}$  merely reflects the growing noise contamination of the data in this low intensity region.<sup>26</sup> (2) Although their relative intensities are not fully understood, the pattern of most of the detailed structure of the mid-IR and far-IR spectra within *ca.*  $45 \text{ cm}^{-1}$  of the band origin is due to transitions between truly bound states, which means that these spectra should provide critical tests of the bound portion of the potential energy surface.

The present work suggests that improvements in our understanding of the partially-resolved IR spectra of N<sub>2</sub>-Ar are likely to arise in the following ways. (1) A more accurate potential energy surface is needed. Note, however, that while full three-dimensional surfaces are certainly desirable to allow proper treatment of collisional inelasticity, our results suggest that an accurate knowledge of the diatom stretching-dependence of the potential surface is not critical to a proper understanding of the partially-resolved IR spectra. After this

work was completed and the manuscript in preparation, a new two-dimensional potential surface for N<sub>2</sub>-Ar was in fact reported by Fernández *et al.*,<sup>28</sup> and we look forward to repeating our calculations to test its ability to predict the mid- and far-IR spectra. (2) A better knowledge of the dipole moment surfaces, including short-range contributions, and a better understanding of the mechanisms driving the mid-IR and far-IR spectra, is required. The key contribution needed here will likely simply be improved calculations of the various N<sub>2</sub> moments and (hyper)polarizabilities. However, it may also be that accurate full *ab initio* dipole moment surfaces will be required. (3) Extending the simulations beyond the truly bound states to include metastable states would certainly be desirable in principle, and would for the first time allow a quantitative explanation of the large amplitude ‘‘ripple structure’’ observed at frequencies lying more than *ca.*  $45 \text{ cm}^{-1}$  from the near- and far-IR band origins.<sup>1-3</sup> However, such calculations would likely have little effect on the quality of the conclusions associated with the better-resolved spectra near the band origins, and would likely not extend significantly our knowledge of the potential or dipole moment surfaces. (4) Obtaining higher resolution experimental far-IR and mid-IR spectra of the complex, with better procedures for reducing background noise and for subtracting the collision-induced background in order to delineate better the actual van der Waals spectra of the complex, would also provide more critical tests of the potential energy and dipole moment surfaces.

## ACKNOWLEDGMENTS

This work was supported by the Natural Sciences and Engineering Research Council (NSERC) of Canada through the award of a NSERC International post-doctoral Fellowship to F.W. and through grants in aid of research to F.R.W.M. and R.J.L. We would like to thank Dr. A. R. W. McKellar for providing the digital representation of his 77 K spectrum, Dr. E. Wishnow and Dr. H. P. Gush for providing digital representations of the experimental far-IR spectrum, and Dr. E. H. Wishnow for useful discussions regarding his far-IR spectrum. We would also like to acknowledge Professor J. Tennyson for providing us with the TRIATOM suite of programs. Finally, F.W. wishes to acknowledge support from Professor F. P. Larkins and The Australian Research Council (ARC).

<sup>1</sup>G. Henderson and G. E. Ewing, *Mol. Phys.* **27**, 903 (1974).

<sup>2</sup>A. R. W. McKellar, *J. Chem. Phys.* **88**, 4190 (1988).

<sup>3</sup>E. H. Wishnow, H. P. Gush, and I. Ozier, *J. Chem. Phys.* **104**, 3511 (1996).

<sup>4</sup>A. G. Ayllón, J. Santamaría, S. Miller, and J. Tennyson, *Mol. Phys.* **71**, 1043 (1990).

<sup>5</sup>F. Wang, F. R. W. McCourt, and R. J. Le Roy, *Mol. Phys.* **88**, 821 (1996).

<sup>6</sup>R. Candori, P. Pirani, and F. Vecchiocattivi, *Chem. Phys. Lett.* **102**, 412 (1983).

<sup>7</sup>W. Jäger, M. C. L. Gerry, C. Bissonnette, and F. R. W. McCourt, *Faraday Discuss. Chem. Soc.* **97**, 105 (1994).

<sup>8</sup>A. Dham, F. R. W. McCourt, and W. J. Meath, *J. Chem. Phys.* **103**, 8477 (1995).

<sup>9</sup>W. Jäger and M. C. L. Gerry, *Chem. Phys. Lett.* **196**, 274 (1992).

<sup>10</sup>J. M. Hutson, in *Advances in Molecular Vibrations and Collision Dynamics*, edited by J. M. Bowman (JAI Press, Greenwich, CT, 1991), Vol. 1A, pp. 1-45.

- <sup>11</sup>G. Brocks and A. van der Avoird, *Mol. Phys.* **55**, 11 (1985).
- <sup>12</sup>R. N. Zare, *Angular Momentum. Understanding Spatial Aspects in Chemistry and Physics* (Wiley-Interscience, New York, 1988).
- <sup>13</sup>J. E. Bohr and K. L. C. Hunt, *J. Chem. Phys.* **86**, 5441 (1987).
- <sup>14</sup>R. J. Le Roy and J. van Kranendonk, *J. Chem. Phys.* **61**, 4750 (1974).
- <sup>15</sup>R. J. Le Roy, G. C. Corey, and J. M. Hutson, *Faraday Discuss. Chem. Soc.* **73**, 339 (1982).
- <sup>16</sup>J. M. Hutson, *J. Chem. Phys.* **96**, 6752 (1992).
- <sup>17</sup>J. M. Hutson, *J. Phys. Chem.* **96**, 4237 (1992).
- <sup>18</sup>J. Tennyson, S. Miller, and C. R. Le Sueur, *Comput. Phys. Commun.* **75**, 339 (1993).
- <sup>19</sup>R. D. Amos, *Mol. Phys.* **39**, 1 (1980).
- <sup>20</sup>H. Hettema, P. E. S. Wormer, and A. J. Thakkar, *Mol. Phys.* **80**, 533 (1993).
- <sup>21</sup>P. W. Fowler, *Chem. Phys. Lett.* **156**, 494 (1989).
- <sup>22</sup>G. Maroulis and D. M. Bishop, *Mol. Phys.* **58**, 273 (1986).
- <sup>23</sup>J. Bendtsen, *J. Raman Spectrosc.* **2**, 133 (1974).
- <sup>24</sup>I. Mills, T. Cvitaš, K. Homann, N. Kallay, and K. Kuchitsu, *Quantities, Units and Symbols in Physical Chemistry*, 2nd ed. (Blackwell Science, Oxford, 1993).
- <sup>25</sup>Recall that the difference between these two dipole moment surfaces is the neglect all of the  $c_{ij}(r_0)$  and  $c'_{ij}(r_0)$  terms in Eqs. (22)–(26) which yields the “pure induction dipole” functions.
- <sup>26</sup>E. H. Wishnow (private communication, 2000).
- <sup>27</sup>To combine these spectra, the frequency zero of the far-IR spectrum was placed at McKellar’s band center (Ref. 2) of  $2429.50\text{ cm}^{-1}$ .
- <sup>28</sup>B. Fernández, H. Kock, and J. Makarewicz, *J. Chem. Phys.* **110**, 8525 (1999).